# Quantitative Morphology Study of Cu-Neutralized Poly(styrene-ran-methacrylic acid) Ionomers: STEM Imaging, X-ray Scattering, and Real-Space Structural Modeling

**ARTICLE** *in* MACROMOLECULES · JANUARY 2007

Impact Factor: 5.8 · DOI: 10.1021/ma0621371



**3 AUTHORS**, INCLUDING:

Nicholas M. Benetatos
U.S. Food and Drug Administration
**11** PUBLICATIONS **93** CITATIONS
SEE PROFILE

Karen I Winey
University of Pennsylvania
**331** PUBLICATIONS **11,291** CITATIONS
SEE PROFILE

# Quantitative Morphology Study of Cu-Neutralized Poly(styrene-*ran*-methacrylic acid) Ionomers: STEM Imaging, X-ray Scattering, and Real-Space Structural Modeling

**Nicholas M. Benetatos,[†] Christopher D. Chan,[‡] and Karen I. Winey*,[†]**

*Department of Materials Science and Engineering and Department of Chemical and Biomolecular Engineering, University of Pennsylvania, Philadelphia, Pennsylvania 19104-6272*

*Received September 14, 2006; Revised Manuscript Received November 18, 2006*

ABSTRACT: Our previous study showed quantitative correspondence between the size of ionic aggregates in a Cu-neutralized poly(styrene-*ran*-methacrylic acid) ionomer (Cu-SMAA) measured from scanning transmission electron microscopy (STEM) images and the sizes determined from X-ray scattering data interpreted using the Yarusso−Cooper model. Here we compare the average sample volume per ionic aggregate ($V_p$) from STEM images and X-ray scattering data from Cu-SMAA. The relationship between the 3D morphology of hard spheres as defined by the Yarusso−Cooper parameters ($R_1$, $R_{CA}$, $V_p$) and the projected 2D images obtained by STEM was elucidated by modeling. These simulations show that a significant number of the ionic aggregates in Cu-SMAA are obscured due to overlap effects and provide a quantitative relationship between the number of spheres in 3D and the number of features in 2D projections as a function of specimen thickness. Upon measuring the local thickness of a Cu-SMAA specimen using electron energy loss spectrometry (EELS), we find that the $V_p$ determined from STEM images strongly agrees with that determined from X-ray scattering data. Thus, quantitative correspondence of both the size and number density of ionic aggregates has been obtained from direct imaging and X-ray scattering of Cu-SMAA. These data provide compelling evidence that the Yarusso−Cooper scattering model presents an excellent description of the nanoscale morphology of this solvent cast ionomer. Interpretation of this morphological data indicates that the ionic aggregates likely include both ionic and nonionic species. This comprehensive characterization provides a foundation on which a systematic evaluation of the factors that influence the nanoscale morphology, and consequently the macroscopic properties, can be accomplished.

## Introduction

For more than a half century, significant research efforts have been devoted toward understanding the processing−structure−property relationships of ionomers. These unique copolymers, in which a small fraction (<10%) of the monomeric units have ionic functionality, exhibit a variety of enhanced properties relative to their homopolymer counterparts including robust mechanical performance and tunable ion transport.[1] The superior properties of ionomers arise from the self-assembly of ionic functional groups and counterions into nanoscale ionic aggregates that act as transient physical cross-links. In order to realize the rational design of ionomers for specific applications, a comprehensive knowledge of the complexities that control the nanometer scale morphology is essential.

Much of the structural information known about ionomers has come from the interpretations of X-ray scattering data. The formation of ionic aggregates manifests itself in the appearance of a broad, isotropic scattering peak in the region between 1 and 5 $nm^{-1}$ and an upturn in scattered X-ray intensity at smaller angles. Despite the inherent difficulty in unearthing structural information from a single broad scattering maximum, several models have been proposed that allow reasonable fitting and interpretation of the data.[2−4] The specific presumptions of these models and the interpretation of SAXS data from ionomers have long been topics of considerable discussion.

The most widely applied ionomer scattering model is that originally proposed by Yarusso and Cooper in 1983.[5] This modified hard-sphere scattering model suggests that the ionomer scattering peak arises from the interparticle interference between ionic aggregates arranged with liquidlike order in the polymer matrix. The spatial correlation in the positions of the ionic aggregates is determined both by the radius of the aggregate and the radius of an excluded volume region surrounding each aggregate that limits the spatial proximity between two scatterers. When these two radii are equal, the Yarusso−Cooper model reduces to that of the hard-sphere liquid derived by Fournet which describes three-body interactions between correlated scatterers.[6] A modified version of the Yarusso−Cooper model was presented by Ding et al.[7] that incorporates the Percus−Yevick total correlation function[8] as solved for the case of a classical hard-sphere liquid.[9,10] This function accounts for correlation between all neighboring particles in the system. Kinning and Thomas found that both correlation functions can provide satisfactory fits to scattering data that exhibit only a single broad peak, as is typical for ionomers; however, the Percus−Yevick correlation function was shown to outperform the Fournet interference function for systems exhibiting high packing densities of hard spheres (>50 vol %).[11] Neither Yarusso−Cooper model interprets the low-angle intensity upturn, as the authors attribute this feature to larger scale inhomogeneities resulting from parasitic scattering such as voids or unreacted neutralizing agent. Subsequent studies have used a variety of methods including anomalous and ultra-small-angle X-ray scattering to gain further insight into the nature of the low-angle upturn and have shown that this zero-order scattering is in fact related to the distribution of ions on length scales on the order of 10−100 nm.[7,12−15]

* To whom correspondence should be addressed. E-mail: winey@seas.upenn.edu.
[†] Department of Materials Science and Engineering.
[‡] Department of Chemical and Biomolecular Engineering.

10.1021/ma0621371 CCC: $37.00 
Published on Web 01/17/2007

Direct imaging of the nanoscale morphology of ionomers has been realized using scanning transmission electron microscopy (STEM).[16,17] The study of ionomers using STEM has revealed a diversity in morphologies on a variety of length scales that, although not entirely unexpected, cannot be explained from SAXS data alone. Ionic aggregates of unexpected shape[18−20] and nonuniform spatial distributions[21,22] have been identified in different systems, though few attempts to comprehensively characterize the nanoscale morphology using a combination of direct imaging and X-ray scattering methods have been performed. Such a study offers the potential to confirm or refute the structural information presupposed from the X-ray scattering model and to establish the domain over which a particular model provides an accurate description of ionomer structure. We have recently conducted a study featuring a solvent cast, Cu-neutralized poly(styrene-*ran*-methacrylic acid) (Cu-SMAA) ionomer.[23] Our results provided the first report of quantitative agreement regarding the *size of the ionic aggregates* as determined from both real-space morphological data, as measured directly by STEM, and reciprocal space scattering data interpreted using the Yarusso−Cooper model.

Here we compare the average sample volume per ionic aggregate, $V_p$, as determined from both imaging and scattering data. Accomplishing this task requires that the local thickness of STEM specimens be precisely measured. We apply electron energy loss spectrometry (EELS) and analyze the low-loss spectrum to determine local specimen thickness. In order to gain additional insight into the morphology observed using STEM, we construct 3D real-space structural models based on our interpretation of the scattering data and simulate 2D projections. The simulation results suggest that particle overlap effects are significant in STEM images of Cu-SMAA. Though the overlap effects do not influence the observed ionic aggregate size, a significant number of aggregates are obscured in projection as the specimen thickness increases. Thus, to accurately determine the number density of ionic aggregates from a STEM image, one must account for all aggregates distributed throughout the specimen volume. Our simulation data provide a specific relationship between the number of features viewed in projection and the number of ionic aggregates in real space as a function of specimen thickness for Cu-SMAA. Incorporating this information into our analysis, the average sample volume per ionic aggregate determined from STEM images of Cu-SMAA strongly agrees with that determined from X-ray scattering data interpreted by the Yarusso−Cooper model. On the basis of this data and the previously reported quantitative description of ionic aggregate size from STEM and X-ray scattering, we conclude that the Yarusso−Cooper scattering model provides an excellent description of the nanoscale morphology of solvent cast Cu-SMAA ionomers.

## Experimental Section

**Materials and Sample Preparation**. A small quantity of copper-(II) acetate monohydrate was dehydrated by heating under vacuum at ∼90−100 °C for 12 h. 28 mg (0.171 mmol) of the dehydrated copper(II) acetate salt was dissolved in methanol (10 mL) and added dropwise to a gently refluxing solution of poly(styrene-*ran*-methacrylic acid) (SMAA) copolymer (7.2 mol % MAA) in toluene (90 mL). The addition of the copper acetate solution was performed over a period of ∼30 min, and the resulting mixture was stirred for 12 h at ∼100 °C. The final solvent ratio was 90/10 toluene/methanol by volume. The Cu-neutralized SMAA ionomer product was isolated by room temperature solvent casting (12 h) and dried under vacuum at ∼90 °C for 12 h to remove volatiles. All materials were stored at room temperature under anhydrous conditions. No additional preparation was necessary for characterization by X-ray scattering.

**X-ray Scattering.** The SAXS apparatus consists of a Nonius FR591 rotating-anode generator operated at 40 kV × 85 mA, mirror−monochromator focusing optics, an evacuated flight path, and a Bruker HiSTAR multiwire two-dimensional detector. Data were acquired over 1 h intervals at a sample−detector distance of 11 cm. The thickness of the solvent cast films ranged between 0.1 and 0.5 mm. 2D data reduction, analysis, and curve fitting were performed using Datasqueeze software.

**Specimen Preparation and STEM.** STEM specimens were sectioned from bulk Cu-SMAA films using a Reichert-Jung ultramicrotome equipped with a diamond knife. Specimen preparation was performed at room temperature with a cutting speed of 0.2−0.4 mm/s and nominal section thickness of 30 nm. STEM and EELS experiments were performed on a JEOL 2010F field emission electron microscope equipped with a Gatan image filter (GIF). The instrument was operated at 197 kV with a 0.7 nm STEM probe and 70 $\mu$m condenser aperture. Images were acquired using a high-angle annular dark field (HAADF) scintillating detector with linear intensity response. The collection angles were 50−110 mrad. EELS spectra were acquired over 5 s intervals.

**Thin Film Preparation.** Polystyrene (PS) films were spin-cast (2000 rpm, 60 s) from solutions (0.5 − 2.0 wt % PS) onto clean Si substrates. The film thicknesses were measured by ellipsometry. Films were floated onto ultrafiltered distilled water, collected atop Cu TEM grids, and dried under vacuum at room temperature.

**Modeling and Simulations.** The program was written in C and compiled using the MinGW C compiler. The random number generator was the MT19337ac algorithm.[24] The program constructs a model where a user-defined volume is filled with hard spheres that have been placed randomly throughout that space according to the parameters specified by the Yarusso−Cooper ionomer scattering model ($R_1$, $R_{CA}$, $V_p$). The simulation imposes periodic boundary conditions. 3D structural data are then converted to intensity by calculating the path length along a *z*-vector using an idealized point STEM probe; here, the contrast between hard spheres and the surroundings is infinite. This was done for the entire volume at 0.1 nm intervals to generate a 2D projected intensity map presented in a six-part color scale. The number of particles in projection was determined by counting features with intensities in the highest 1/3 of cumulative projected intensity. Reported numbers represent the mean as determined from five simulated structures for each user-defined volume.

## Results and Discussion

**STEM and X-ray Scattering from Cu-SMAA**. The size of ionic aggregates in Cu-SMAA has been previously investigated using a combination of STEM and X-ray scattering.[23] Figure 1a depicts the intensity of scattered X-rays as a function of scattering vector, $q = 1.6-16$ nm$^{-1}$. The pattern shows three broad, isotropic peaks: the "ionomer" peak (3.7 nm$^{-1}$), the "polymerization" peak (7 nm$^{-1}$), and the amorphous halo (13 nm$^{-1}$). The ionomer peak confirms the presence of ionic aggregates while the polymerization peak and amorphous halo are typical features in the scattering patterns of PS homopolymer and unneutralized SMAA copolymers.[25−27]

As previously reported, the scattering data from Cu-SMAA were modeled using the following empirical functional form:

$$I(q) = I_{YC}(q) + L_1(q) + L_2(q) + C \qquad (1)$$

where $I_{YC}(q)$ is the original Yarusso−Cooper ionomer scattering model[5] (Fournet correlation term) used to interpret the ionomer peak, $L_1(q)$ and $L_2(q)$ are Lorentzian functions used to describe the sample-derived background, and $C$ is a constant to account for the experimental background. As applied here, the Yarusso−Cooper model has four independent fitting parameters: the ionic aggregate radius $R_1$, the radius of closest approach $R_{CA}$ that

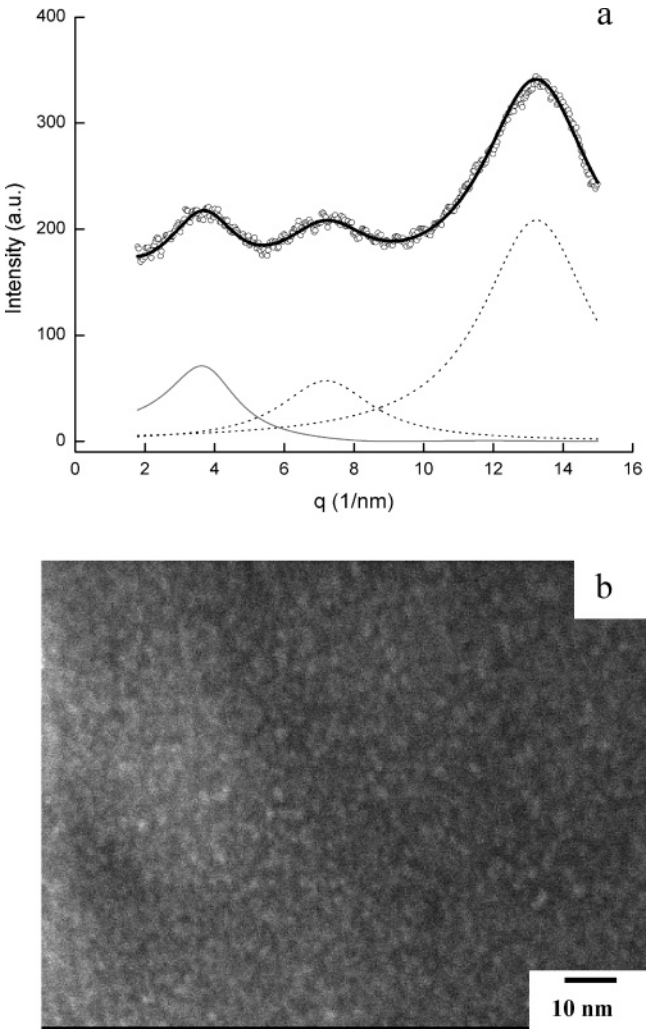


**Figure 1.** (a) Scattered intensity as a function of scattering vector, $q$, for Cu-SMAA along with the best-fit model (solid). Our empirical model includes the Yarusso−Cooper model for interparticle scattering from spherical ionic aggregates (gray), two Lorentzian functions (dotted), and an additive constant. (b) HAADF STEM image of Cu-SMAA shows a dense, uniform distribution of Cu-rich features.

limits the spatial correlation between two aggregates, the average sample volume per aggregate $V_p$, and the peak amplitude $A$ which incorporates all of the factors affecting the absolute value of intensity. A least-squares regression[28] optimized the independent fitting parameters of each subfunction and generated the best-fit curve, which is shown in comparison with the scattering data (Figure 1a). These scattering results interpreted with our empirical model indicate the presence of a uniform distribution of monodisperse, spherical ionic aggregates with a diameter ($D = 2R_1$) of 1.0 nm, a minimum closest approach distance between centers ($D_{CA} = 2R_{CA}$) of 1.4 nm, and average sample volume per ionic aggregate ($V_p$) of 4−8 nm$^3$/particle. A range is given for $V_p$ based on fitting absolute intensity scattering data (see Supporting Information).

Using HAADF STEM, we have imaged these nanoscale ionic aggregates in thin specimens sectioned from the same bulk Cu-SMAA ionomer characterized by X-ray scattering. The bright features visible in the image of Figure 1b correspond to areas of higher average atomic number (i.e., Cu-rich aggregates) within a matrix of lower average atomic number. The Cu-rich aggregates appear spherical, monodisperse, and distributed uniformly throughout the specimen. The average diameter of the ionic aggregates, measured via methods described in a previous study,[29] was determined as 1.2 ± 0.3 nm. Here the error is the standard deviation of 40 individual measurements, corresponding to an uncertainty of <2 pixels per ionic aggregate. Thus, our STEM results are consistent with a monodisperse size distribution of ionic aggregates convoluted with finite instrumental resolution.

For this particular ionomer sample, both imaging and scattering data indicate uniformly distributed, monodisperse, spherical ionic aggregates with diameters of ∼1.0 nm, suggesting that the Yarusso−Cooper model provides an excellent description of ionic aggregate size in Cu-SMAA. Next, we investigate the average sample volume per ionic aggregate using both STEM and scattering data. This analysis requires the local thickness of STEM specimens to be quantitatively determined.

**Determining Local Specimen Thickness**. Several experimental techniques exist that allow the approximation of TEM specimen thickness including the analysis of convergent beam diffraction patterns, creating surface features and tilting the specimen to observe their lateral translation, and measuring the bremsstrahlung continuum from an X-ray emission spectrum.[30] These methods require either crystalline specimens or conditions that are unfavorable to analyzing polymeric materials such as high electron dose and local beam damage. Electron energy loss spectrometry (EELS) provides an attractive means of measuring local thickness in situ without compromising the ability to image the specimen at high magnification. This technique uses a magnetic prism to separate the transmitted electrons based on the amount of energy lost due to inelastic scattering events within the specimen.

Typical EELS spectra consist of a zero-loss peak, low-loss region, and high-loss region. The zero-loss peak arises from electrons that have been scattered elastically, i.e., have not lost energy while interacting with the specimen. The low-loss region provides information from electrons that have interacted with weakly bound, outer-shell electrons in the specimen typically producing plasmon oscillations. The high-loss region, which is significantly less intense relative to the zero-loss peak and the low-loss region, results from inelastic interactions with inner shell, core electrons of the specimen. It is these inelastic events that provide detailed information regarding the chemical nature, bonding, and composition of the specimen.

Information pertaining to the specimen thickness is contained within the EELS spectrum. By taking the ratio of the intensity under the total energy loss spectrum ($I_T$), as obtained by integration, to the intensity under the zero-loss peak ($I_0$), the thickness ($t$) may be estimated in terms of the inelastic mean free path ($\lambda_I$) using the following relation:

$$t = \lambda_I \ln\left(\frac{I_T}{I_0}\right) \tag{2}$$

Thus, the local specimen thickness ($t$) can be determined, when the inelastic mean free path of the material is known under the appropriate experimental conditions. Using this method, the thickness of a specific area can be measured rather quickly during STEM imaging to within ∼20% error,[31] providing the information needed to estimate the average volume occupied by individual ionic aggregates.

To approximate $\lambda_I$ for our Cu-SMAA ionomers under our imaging conditions, we perform EELS analysis on spin-cast PS homopolymer films, where the film thicknesses were predetermined. The films were spin-cast on Si substrates, measured with ellipsometry, and transferred to TEM grids. Because the thickness of the PS films was known a priori, an average inelastic mean free path was computed for each film using eq

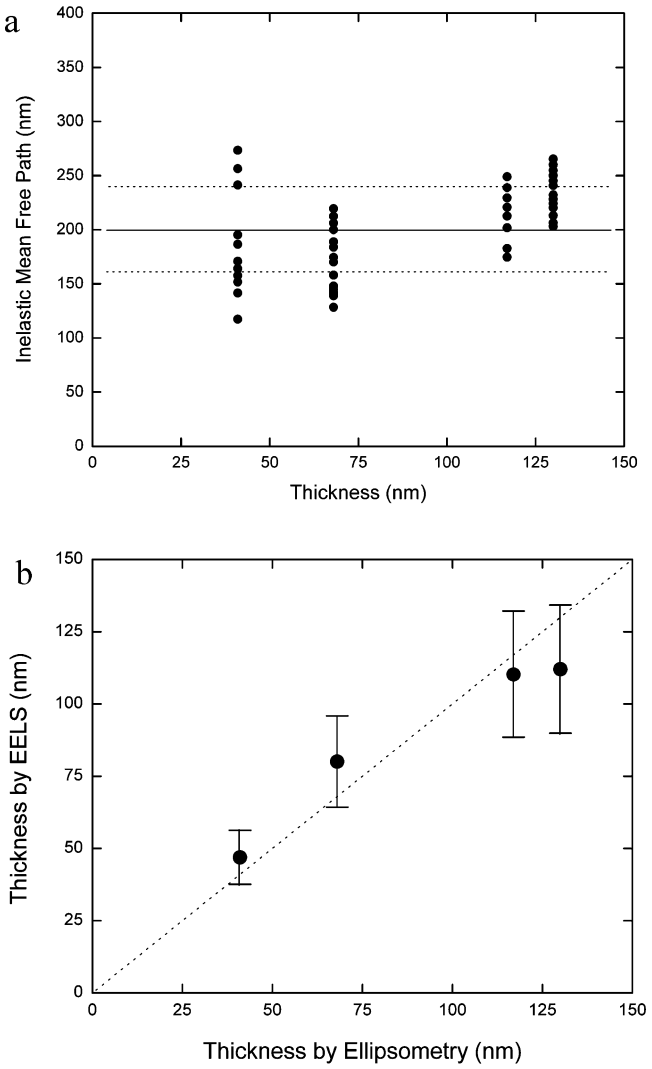


**Figure 2.** **(a)** Inelastic mean free path calculated from PS films of predetermined thicknesses (41, 68, 117, 130 nm). Solid line depicts the average inelastic mean free path of 200 nm, while the standard deviation of ±20% is shown by the dashed lines. **(**b**)** Film thickness as determined by the EELS log ratio method based on the average inelastic mean free path. Dashed line represents equivalent thickness values from both characterization methods. To within the uncertainty displayed by the error bars, thickness measurements using EELS are consistent with ellipsometry data.

2. Figure 2a depicts the value of $\lambda_I$ determined via EELS for spin-cast PS films of four different thicknesses from 40 to 130 nm. Multiple (10−15) measurements of $\lambda_I$ were performed under identical imaging conditions (197 kV, 0.7 nm STEM probe, and 70 $\mu$m condenser aperture) for each film. From EELS data of all four films, we determine an average inelastic mean free path of 200 ± 40 nm. This value is consistent with inelastic mean free path data for PS measured between 0.05 and 2 keV and extrapolated to higher incident electron energy (197 keV).[32−35] Using our average $\lambda_I$, subsequent thickness measurements were made on new grids containing each of the PS films, and the measured values were compared with those determined from ellipsometry. Figure 2b illustrates that the local thickness of PS determined via EELS agrees with ellipsometry data to within the error of the inelastic mean free path.

**Average Sample Volume per Ionic Aggregate.** The thickness of the Cu-SMAA ionomer specimen (from which the image of Figure 1b was acquired) was determined via the EELS log ratio method, eq 2. The thickness ($t$) was found to be 72 ± 15 nm, and the number of features in a 25 × 25 nm area ($A$) of the STEM images ranged between 125 and 175. Assuming a one-to-one correspondence between the number of features in a 2D STEM image ($N_{2D}$) and the number of ionic aggregates in the specimen volume ($N_{3D}$), i.e., assuming no overlap, we determine an average sample volume per ionic aggregate as follows:

$$V_{\text{p without overlap}} = \frac{At}{N_{3D}} \sim \frac{At}{N_{2D}} = 204 - 435 \quad \frac{\text{nm}^3}{\text{particle}} \quad (3)$$

This surprisingly large volume per particle ($V_p$) is inconsistent with the experimentally observed interparticle scattering and would likely give rise to only form factor scattering from nanoscale spheres. In contrast, the $V_p$ obtained from our X-ray scattering data fit with our empirical model is 4−8 nm$^3$/particle. Thus, the assumption of zero particle overlap and a straight forward one-to-one correspondence between $N_{2D}$ and $N_{3D}$ is not valid.

In order to explore the relationship between $N_{2D}$ and $N_{3D}$, a computational model was developed that constructs a real-space depiction of the structure of Cu-SMAA as given by the Yarusso−Cooper scattering model. The computational model sequentially places hard spheres of radius $R_1$ at random positions within a volume and removes any sphere less than $2R_{CA}$ center-to-center distance from an existing sphere. The number of hard spheres inserted into the volume, $N_{3D}$, is specified by the total volume, $V$, and $V_p$ as determined from the scattering data. Figure 3a depicts a volume 25 nm in length, 25 nm in width, with thickness of 1 nm (total volume $V = 625$ nm$^3$) that has been randomly populated with hard spheres. The characteristics of the spheres are given by the best fit parameters from the X-ray scattering of Cu-SMAA interpreted with the Yarusso−Cooper model: $2R_1 = 1.0$ nm, $2R_{CA} = 1.5$ nm, and $V_p = 5$ nm$^3$/particle. For the structure depicted in Figure 3a, the total number of spheres, $N_{3D}$, is 125.

From this real-space model, we create a 2D intensity plot from the hard spheres, Figure 3b, in which the intensity of a hard sphere in projection is given by

$$I(x) = 2x \tan\left[\cos^{-1}\left(\frac{x}{R_1}\right)\right] \quad (4)$$

where $R_1$ is the radius of the hard sphere and $x$ is the shortest distance from the projection vector to the center of the sphere. The projected intensity of all spheres contained within the volume ($V$) is visually depicted by a color scale partitioned into six equal fractions. In this idealized case where the simulated specimen thickness is equal to the diameter of the sphere ($t = 2R_1 = 1$ nm), the intensity of the projected spheres scales rapidly to the highest intensity level (red) while unoccupied areas have zero intensity (blue). Figure 3c shows a line scan of projected intensity across the intensity map at the location illustrated by the white line in Figure 3b. Only a line scan across the geometric center of a sphere has the maximum intensity and a width equal to the sphere diameter. The off-diameter line scans have both lower intensity and smaller widths (Figure 3c). In this case, the number of objects visible in the 2D projection (125) is equal to the number of objects in the real-space volume (125) as the thickness of the simulated volume prohibits sphere overlap.

Increasing the thickness by a factor of 5, simulating the 3D structure (Figure 4a), and projecting it into 2D (Figure 4b) gives rise to several interesting results. In this case, particle overlap occurs and the projected intensity map is more complex than that of the simple monolayer case. The regions of the intensity map that exhibit the highest cumulative intensity level (red)

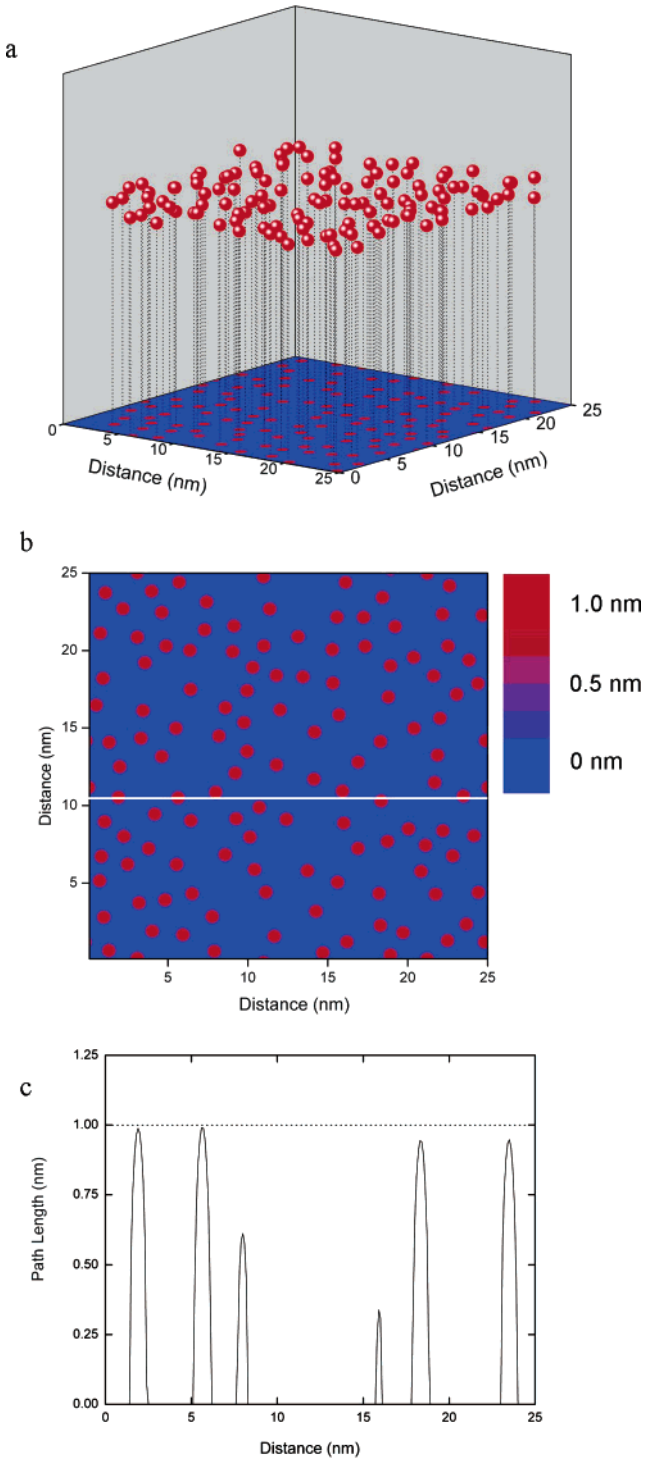


**Figure 3.** **(a)** 3D real-space volume (25 × 25 × 1 nm$^3$) randomly populated with hard spheres ($R_1$ = 1.0 nm, $R_{CA}$ = 0.75 nm, and $V_p$ = 5 nm$^3$/particle). **(b)** Projected intensity map of the structure depicted in (a). **(c)** Projected intensity from the solid white line depicted in (b).

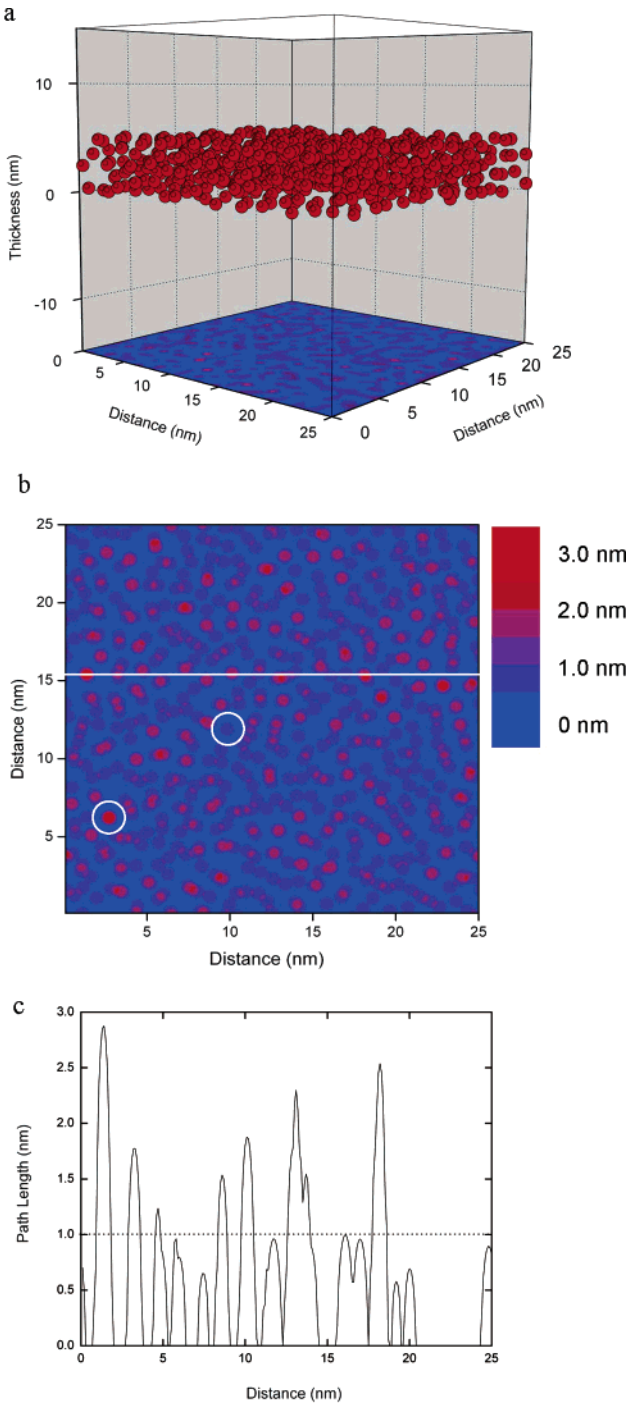


**Figure 4.** **(a)** 3D real-space volume (25 × 25 × 5 nm$^3$) randomly populated with hard spheres ($R_1$ = 1.0 nm, $R_{CA}$ = 0.75 nm, and $V_p$ = 5 nm$^3$/particle). **(b)** Projected intensity map of the structure depicted in (a). Circles illustrate a region of high cumulative overlap (red) and a nonoverlapped, isolated particle (dark blue). **(c)** Projected intensity from the solid white line depicted in (b).

correspond to areas where three or more spheres have overlapped; the cumulative projected intensity of these regions is ≥3 particle diameters. An isolated sphere with diameter of 1.0 nm appears dark blue on this projected intensity scale. Examples of these two extreme cases are indicated in Figure 4b. The concept is further illustrated by a line scan across the 2D intensity map (Figure 4c); the individual particle diameter of 1 nm has been indicated with a dashed line. It should be noted that the width of the intensity profile for the regions of highest cumulative overlap does not significantly differ from that of an isolated nonoverlapped sphere, as the centers of the spheres must align to maximize the total projected intensity. One of the advantages of STEM imaging is that the STEM detectors allow manipulation of the digital signal to accentuate the highest intensity regions at the expense of lower intensity areas. It is expected that, for a densely populated system, the areas of highest cumulative overlap are preferentially imaged.

The number of red features visible in the 2D intensity map projected from a 5 nm thick volume is 150 ± 6 (Figure 4b). This is only marginally greater than the number visible in the monolayer case in which $N_{2D}$ ($t$ = 1 nm) = 125; however, the actual number of spheres in real space (Figure 4a) has increased

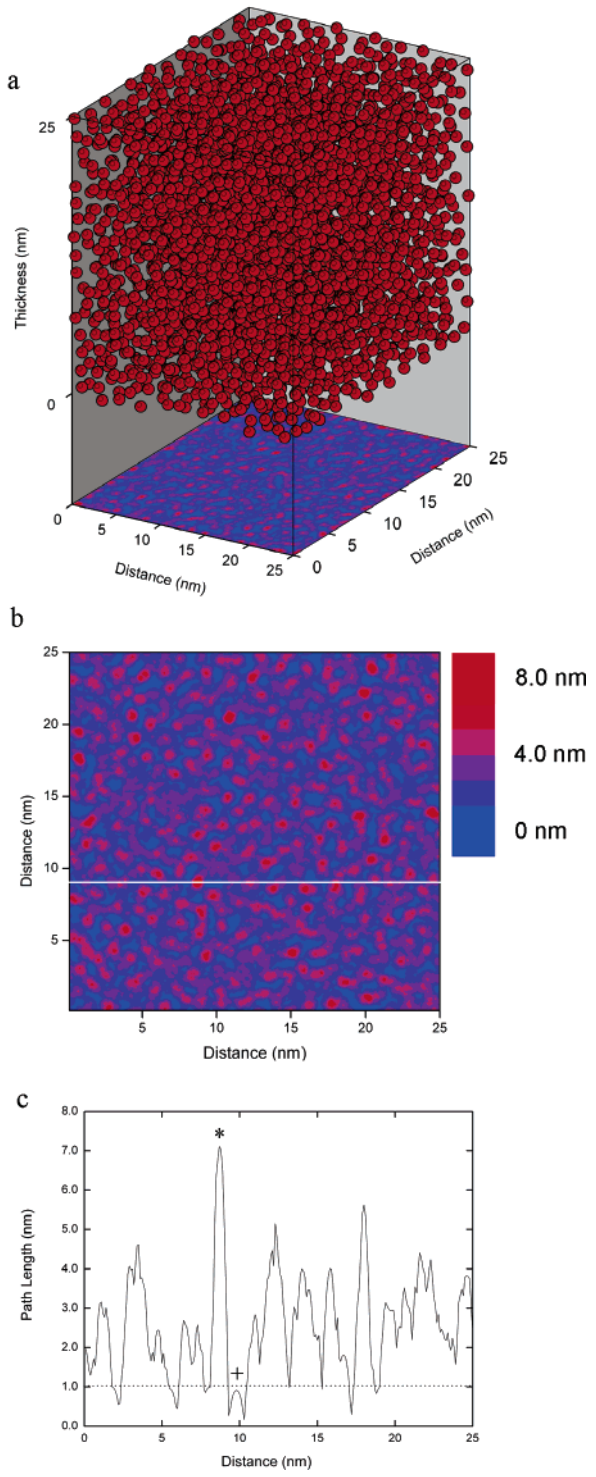


**Figure 5.** **(a)** 3D real-space volume ($25 \times 25 \times 25$ nm$^3$) randomly populated with hard spheres ($R_1 = 1.0$ nm, $R_{CA} = 0.75$ nm, and $V_p = 5$ nm$^3$/particle). **(b)** Projected intensity map of the structure depicted in (a). **(c)** Projected intensity from the solid white line depicted in (b). Note that projected features have similar diameter in both the case of ~7 overlapping spheres (*) and 1 isolated sphere (+).

5-fold. As the thickness of the simulated specimen increases, the contribution of particle overlap becomes significant and the number of features visible in projection substantially underestimates the number of objects in the 3D volume. For example, at a thickness of 5 nm the ratio $N_{2D}/N_{3D}$ is 0.24.

Figures 5a and 5b illustrate similar results for a thickness of 25 nm. Here the regions of highest cumulative intensity overlap represent ≥8 overlapping spheres. Note the similarities between

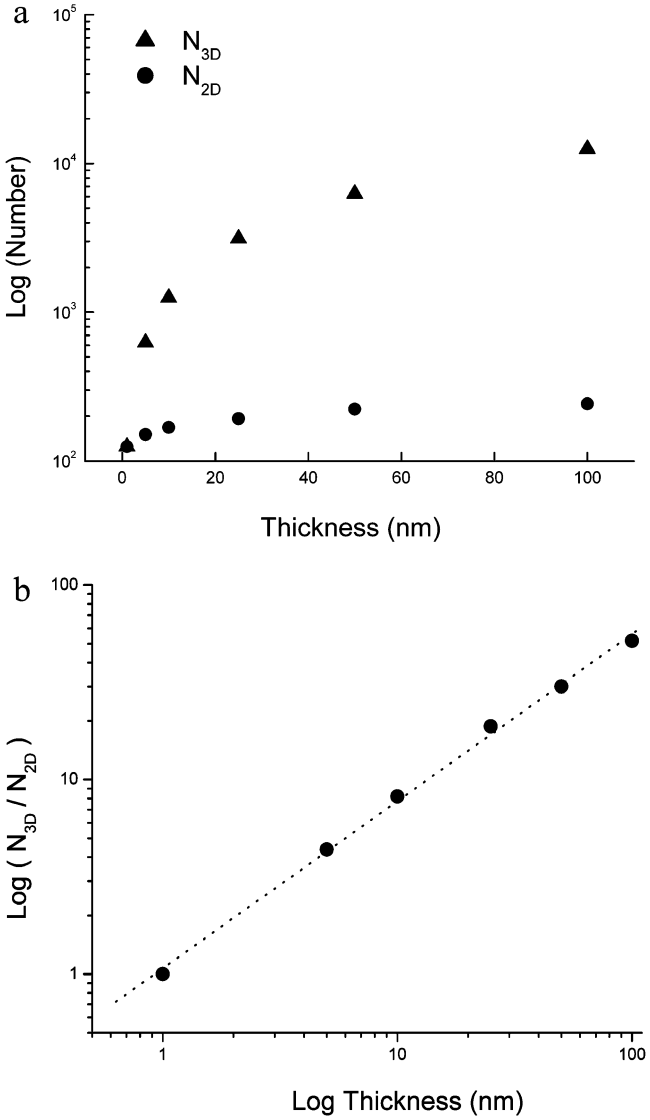


**Figure 6.** (a) Semilogarithmic scale plot depicts the increasing contribution of particle overlap with increasing specimen thickness. As the specimen thickness approaches typical experimental values (50−100 nm), $N_{2D}$ (●) significantly underestimates $N_{3D}$ (▲). (b) Values of $N_{3D}/N_{2D}$ (●) as a function of thickness and line of best fit (dotted) plotted on a logarithmic scale. Linear slope ($m = 0.9$) indicates a power law relationship between $N_{3D}/N_{2D}$ and the specimen thickness for the specific parameters of this simulation.

Figures 1b and 5b in feature size, shape, and areal density. The number of red features visible in projection in Figure 5b is 193 ± 8, a quantity that represents only ~5% of the number of spheres present in the real-space volume. A line scan of the projected intensity emphasizes the enormous effect of particle overlap, illustrating a minimum "background" of ~1 particle across the intensity map (Figure 5c). Despite significant overlap effects, the width of the high-intensity regions remains consistent with that of an isolated sphere. As the simulated thickness approaches typical experimental values (40−100 nm), the 2D projections depict only 2−3% of the particles occupying the 3D volume (Figure 6a).

We have created real-space depictions of the specific nanoscale morphology of Cu-SMAA as defined by the Yarusso−Cooper scattering model. From these we have constructed projections that are consistent with our STEM images. These data suggest that in STEM specimens of Cu-SMAA, which are densely populated with ionic aggregates, the effect of particle

overlap is significant. To estimate $N_{3D}$ using $N_{2D}$ from STEM images, we have plotted the ratio $N_{3D}/N_{2D}$ from the simulations as a function of thickness (Figure 6b). Plotting the data in this manner, we identify a power law relationship for Cu-SMAA between $N_{3D}/N_{2D}$ and the simulated specimen thickness ($t$):

$$N_{3D} = N_{2D}t^{0.9} \tag{5}$$

Interestingly, $N_{3D}$ is roughly proportional to $t$, indicating that the 2D projection approximates that of a monolayer (i.e., independent of thickness) for this specific simulated morphology. Applying this relationship for Cu-SMAA to the STEM data presented above ($N_{2D}$, $t$), we determine $V_p$ as follows:

$$V_{p\ \text{with overlap}} = \frac{At}{N_{3D}} = \frac{At}{N_{2D}t^{0.9}} = 5.3 - 7.8 \quad \frac{\text{nm}^3}{\text{particle}} \tag{6}$$

This value of $V_p$ is perfectly consistent with that determined from our X-ray scattering data (4−8 nm$^3$/particle).

The quantitative correspondence of both the size and number density of ionic aggregates obtained from direct imaging and X-ray scattering of Cu-SMAA provides compelling evidence that the Yarusso−Cooper scattering model presents an excellent description of the nanoscale morphology of this ionomer, prepared under a particular set of conditions. These data constitute the most comprehensive characterization of the nanoscale morphology of an ionomer to date and provide a foundation on which future studies can systematically explore how the many variables relevant in the synthesis, preparation, and processing of ionomers influence the nanoscale morphology and, consequently, the bulk properties. In addition, the domain over which the Yarusso−Cooper model describes the morphology within SMAA ionomers and subsequently for other ionomer materials can be established.

**Discussion of Aggregate Composition**. A well-established model of ionomer morphology is that originally proposed in 1990 by Eisenberg, Hird, and Moore (EHM).[1,36] The EHM model postulates two types of ionic aggregation termed *multiplets* and *clusters*. A *multiplet* is defined as a small group of exclusively ion pairs surrounded by a layer of hydrocarbon, the segmental mobility of which is restricted relative to that of the bulk polymer. Assumed to be spherical, geometric limitations based on the size of ion pairs suggest multiplets are on the order of 1.0 nm or less in diameter. Similarly, the Yarusso−Cooper scattering model describes a spherical ion-rich core of radius $R_1$ surrounded by a layer with electron density equal to that of the polymer matrix that limits the extent to which scatterers can pack together to a minimum distance of $2R_{CA}$ between centers. *Clusters* are defined as collections of *multiplets* wherein the restricted mobility layer in the immediate vicinity is postulated to be large enough (∼5−10 nm) to exhibit its own glass transition temperature. This model has been used to interpret a large body of experimental data pertaining to the chain dynamics of ionomers. Despite its widespread application, direct experimental corroboration of the postulated morphology of the EHM model is largely lacking.

While the size of the ionic aggregates in Cu-SMAA determined using X-ray scattering and STEM imaging is consistent with that predicted for multiplets, the EHM model argues that the composition of a multiplet is entirely ionic and excludes polymer chain. We can evaluate this hypothesis by calculating the number of acid−counterion pairs that can pack into an ionic aggregate of radius ($R_1$) and comparing it with the number of ion pairs in $V_p$ determined from the global composition of the acid copolymer. The comparison will provide insight into the validity of assuming a 100% ionic composition of the ionic aggregates.

To determine the number of acid−counterion pairs in an ionic aggregate from $R_1$, we estimate that the coordination structure of each pair is similar to that of the copper(II) acetate salt. This approach has previously been described.[37] Thus, the volume occupied by an acid−counterion pair ($Cu^{2+}[COO^-]_2$) can be estimated using the density ($\rho_{acetate} = 1.88 \times 10^{-21}$ g/nm$^3$) and molar mass ($M_{acetate} = 181.59$ g/mol) of dehydrated copper(II) acetate, scaled by the number of atoms in the acid−counterion pair ($n_{ion\ pair} = 2\ C + 4\ O + 1\ Cu = 7$ atoms) relative to the total number of atoms in the acetate salt ($n_{acetate} = 4\ C + 6\ H + 4\ O + 1\ Cur = 15$ atoms). Using this method, the volume of an acid−counterion pair is given by the following:

$$V_{ion\ pair} = \frac{n_{ion\ pair}}{n_{acetate}}\left(\frac{M_{acetate}}{N_A\rho_{acetate}}\right) \tag{7}$$

where $N_A$ is Avogadro's number. Assuming that the ionic aggregate is entirely composed of ionic material confined within the volume defined by the aggregate radius, the total number of cations ($N_{cation}$) can be calculated as follows:

$$N_{cation,R_1} = \frac{{}^4/_3\pi {R_1}^3}{V_{ion\ pair}} \tag{8}$$

The result for Cu-SMAA is that ∼7 cations can occupy the ionic aggregate.

Independently, the number of cations per $V_p$ is calculated from knowledge of the acid copolymer composition. For Cu-SMAA, $V_p$ ranges between 4 and 8 nm$^3$ per aggregate. The composition of the SMAA copolymer is 93 mol % PS and 7 mol % MAA. The volume fraction of acid groups ($\phi_{MAA}$) can be estimated using the homopolymer densities and molar mass of polystyrene ($\rho_{PS} = 1.05 \times 10^{-21}$ g/nm$^3$ and $M_{PS} = 104$ g/mol) and poly(methacrylic acid) ($\rho_{MAA} = 1.28 \times 10^{-21}$ g/nm$^3$ and $M_{MAA} = 85$ g/mol), as follows:

$$\phi_{MAA} = \frac{m_{MAA}\left(\frac{M_{MAA}}{\rho_{MAA}}\right)}{(1 - m_{MAA})\frac{M_{PS}}{\rho_{PS}} + m_{MAA}\frac{M_{MAA}}{\rho_{MAA}}} = 0.05 \tag{9}$$

where $m_{MAA}$ is the mole fraction of methacrylic acid in the copolymer. We also determine the number of methacrylic acids per unit volume ($\eta_{MAA}$):

$$\eta_{MAA} = \left(\frac{\rho_{MAA}}{M_{MAA}}\right)N_A = 9\ \frac{\text{MAA units}}{\text{nm}^3} \tag{10}$$

Using this quantity, along with the volume fraction of acid groups and the average sample volume per particle ($V_p$), we determine the average number of ion pairs that can occupy one $V_p$ of sample:

$$N_{cation,V_p} = \frac{1}{2}\phi_{MAA}V_p\eta_{MAA} \tag{11}$$

From eq 11 we calculate that only 2−4 cations can occupy the volume defined by $V_p$ based on the known composition of the SMAA copolymer. In contrast, eq 8 indicates that each ionic aggregate can accommodate ∼7 cations. Thus, for this particular

copolymer composition, the ionic aggregates apparently do not consist of purely ionic material, as per the assumption of the EHM model. Although each ionic aggregate could accommodate ~7 cations based on $R_1$, the separation between ionic aggregates as defined by $V_p$ indicates less than half that number. Therefore, the ionic aggregates likely include a combination of both ionic material *and* hydrocarbon.

The data presented here constitute the most rigorous characterization of ionomer morphology on the nanoscale to date. The data have provided new insight as to the nature and the composition of the ionic aggregates and encourage future studies to explicitly quantify the relationships between the complex morphologies of ionomers and the macroscopic properties. Systematic studies that highlight the role of copolymer chemical structure, counterion type, processing methods, etc., will provide valuable insight regarding the parameters necessary for the design, synthesis, and preparation of improved ionomeric materials.

## Conclusion

We have rigorously investigated the nanoscale morphology of Cu-SMAA using a combination of direct imaging, scattering, and real-space structural modeling. The ionic aggregate sizes determined from model-independent STEM imaging and scattering data interpreted by the Yarusso−Cooper model are in strong agreement. Direct imaging and scattering characterization methods both indicate uniformly distributed, spherical ionic aggregates with diameters of ~1.0 nm.

Overlap in STEM images was modeled by constructing a volume containing hard spheres according to the criteria of the Yarusso−Cooper scattering model. The simulated 2D projections show that a significant number of the ionic aggregates in STEM images of Cu-SMAA are obscured due to overlap effects and that only the regions of highest cumulative intensity are likely visualized. These regions are similar in size to the hard spheres but represent only a fraction of the number present in 3D. The simulations provide a quantitative relationship between the number of spheres in a volume and the number of features in a projected area as a function of thickness. Thus, upon measuring the thickness of Cu-SMAA STEM specimen using the EELS log ratio method, the average sample volume per ionic aggregate was determined (5−8 $nm^3$/particle) and found to agree with the scattering data interpreted by the Yarusso−Cooper model (4−8 $nm^3$/particle).

These data for the size and number density of ionic aggregates in Cu-SMAA provide strong testament that the Yarusso−Cooper scattering model accurately describes the morphology of this ionomer. We have used this morphological data to estimate the composition of the ionic aggregates and found that the ionic aggregates in Cu-SMAA are likely to include both ionic pairs and hydrocarbon segments. This level of morphological data encourages new contemplation regarding the nature and composition of nanometer scale ionomer morphology and new investigation of methods to manipulate these structures to design materials with improved properties.

**Acknowledgment.** Funding was provided by the National Science Foundation (DMR02-35106 and DMR05-20020). The authors gratefully acknowledge Prof. Joon-Seop Kim of Chosun University for providing SMAA copolymers and Prof. Russell Composto for the use of the ellipsometer. We also acknowledge Prof. Paul A. Heiney, Prof. David E. Luzzi, and Dr. Doug Yates for helpful discussions along with Dr. Frederick Beyer, who provided technical assistance regarding the absolute intensity calibration of scattering data. Glassy carbon standards were provided by Dr. Jan Ilavsky of Argonne National Laboratories. Nicholas M. Benetatos acknowledges funding provided through an Augustus T. Ashton fellowship at the University of Pennsylvania.

**Supporting Information Available:** Modeling of scattering data from Cu-SMAA. This material is available free of charge via the Internet at http://pubs.acs.org.

## References and Notes

(1) Eisenberg, A.; Kim, J.-S. *Introduction to Ionomers*; John Wiley & Sons: New York, 1998.
(2) MacKnight, W. J.; Taggart, W. P.; Stein, R. S. *J. Polym. Sci., Polym. Symp.* **1974**, *45*, 113−128.
(3) Marx, C. L.; Caulfield, D. L.; Cooper, S. L. *Macromolecules* **1973**, *6*, 344−353.
(4) Roche, E. J.; Stein, R. S.; Russell, T. P.; MacKnight, W. J. *J. Polym. Sci., Polym. Phys. Ed.* **1980**, *18*, 1497−1512.
(5) Yarusso, D.; Cooper, S. L. *Macromolecules* **1983**, *16*, 1871−1880.
(6) Fournet, G. *Acta Crystallogr.* **1951**, *4*, 293−301.
(7) Ding, Y. S.; Hubbard, S. R.; Hodgson, K. O.; Register, R. A.; Cooper, S. L. *Macromolecules* **1988**, *21*, 1698−1703.
(8) Percus, J. K.; Yevick, G. J. *Phys. Rev.* **1958**, *110*, 1−13.
(9) Thiele, E. J. *J. Chem. Phys.* **1963**, *39*, 474.
(10) Wertheim, M. S. *Phys. Rev. Lett.* **1963**, *10*, 321.
(11) Kinning, D. J.; Thomas, E. L. *Macromolecules* **1984**, *17*, 1712−1718.
(12) Chu, B.; Wu, D. Q.; Lundberg, R. D.; MacKnight, W. J. *Macromolecules* **1993**, *26*, 994−999.
(13) Chu, B.; Wu, D. Q.; MacKnight, W. J.; Wu, C.; Phillips, J. C.; LeGrand, A.; Lantman, C. W.; Lundberg, R. D. *Macromolecules* **1988**, *21*, 523−525.
(14) Wu, D. Q.; Chu, B.; Lundberg, R. D.; MacKnight, W. J. *Macromolecules* **1993**, *26*, 1000−1007.
(15) Wu, D. Q.; Phillips, J. C.; Lundberg, R. D.; MacKnight, W. J.; Chu, B. *Macromolecules* **1989**, *22*, 992−995.
(16) Laurer, J. H.; Winey, K. I. *Macromolecules* **1998**, *31*, 9106−9108.
(17) Winey, K. I.; Laurer, J. H.; Kirkmeyer, B. P. *Macromolecules* **2000**, *33*, 507−513.
(18) Batra, A.; Cohen, C.; Kim, H.; Winey, K. I.; Ando, N.; Gruner, S. M. *Macromolecules* **2006**, *39*, 1630−1638.
(19) Kirkmeyer, B. P.; Taubert, A.; Kim, J.-S.; Winey, K. I. *Macromolecules* **2002**, *35*, 2648−2653.
(20) Kirkmeyer, B. P.; Weiss, R. A.; Winey, K. I. *J. Polym. Sci., Part B: Polym. Phys.* **2001**, *39*, 477−483.
(21) Benetatos, N. M.; Winey, K. I. *J. Polym. Sci., Part B: Polym. Phys.* **2005**, *43*, 3549−3554.
(22) Taubert, A.; Winey, K. I. *Macromolecules* **2002**, *35*, 7419−7426.
(23) Benetatos, N. M.; Heiney, P. A.; Winey, K. I. *Macromolecules* **2006**, *39*, 5174−5176.
(24) Matsumoto, M.; Nishimura, T. *ACM Trans. Model. Comput. Simul.* **1998**, *8*, 3−30.
(25) Ayyagari, C.; Bedrov, D.; Smith, G. D. *Macromolecules* **2000**, *33*, 6194−6199.
(26) Mitchell, G. R.; Windle, A. H. *Polymer* **1984**, *25*, 906−920.
(27) Wecker, S. M.; Davidson, T.; Cohen, J. B. *J. Mater. Sci.* **1972**, *7*, 1249−1259.
(28) Heiney, P. A. *Comm. Powder Diffr. Newsletter* **2005**, *32*, 9−11.
(29) Benetatos, N. M.; Smith, B. W.; Heiney, P. A.; Winey, K. I. *Macromolecules* **2005**, *38*, 9251−9257.
(30) Egerton, R. F. *Electron Energy Loss Spectroscopy in the Electron Microscope*, 2nd ed.; Plenum Press: New York, 1996.
(31) Malis, T. *J. Electron Microsc. Tech.* **1988**, *8*, 193−200.
(32) Cumpson, P. J. *Surf. Interface Anal.* **2001**, *31*, 23−34.
(33) Tanuma, S.; Powell, C. J.; Penn, D. R. *Surf. Interface Anal.* **1988**, *11*, 577.
(34) Tanuma, S.; Powell, C. J.; Penn, D. R. *Surf. Interface Anal.* **1991**, *17*, 911−926.
(35) Tanuma, S.; Powell, C. J.; Penn, D. R. *Surf. Interface Anal.* **1991**, *17*, 927.
(36) Eisenberg, A.; Hird, B.; Moore, R. B. *Macromolecules* **1990**, *23*, 4098−4107.
(37) Grady, B. P.; Floyd, J. A.; Genetti, W. B.; Vanhoorne, P.; Register, R. A. *Polymer* **1999**, *40*, 283−288.

MA0621371